AIMS Energy

http://www.aimspress.com/journal/energy

AIMS Energy, 8(2): 214–230.
DOI: 10.3934/energy.2020.2.214
Received: 06 November 2019
Accepted: 21 February 2019
Published: 13 March 2020

Research article

Power dispatching techniques as a finite state machine for a standalone photovoltaic system with a hybrid energy storage

K.M.S.Y. Konara *, M.L. Kolhe and Arvind Sharma

Faculty of Engineering & Science, University of Agder, Centre for Integrated Emergency Management, PO Box 422, NO 4604, Kristiansand, Norway

* **Correspondence:** Email: konara@uia.no.

Abstract: Standalone photovoltaic system (SPVS) is usually embedded with an energy storage unit to overcome the intermittency of photovoltaic (PV) generation as well as to address load variations in off-grid operation. In SPVS energy systems, batteries can serve as the long term energy storage and contributing to the large portion of the energy demand but to overcome the load intermittency, it necessitates a fast response energy storage embedded with the battery as a hybrid energy storage (HES) for dynamic loads (e.g., Electric Vehicle loads, emergency power management). In this work, Lead-Acid (LA) battery and supper capacitor (SC) array are used as the HES. HES helps not only in increasing more utilization of PV generated power but also in improving system dynamics and stability for power intensive loads operation. This paper presents innovative power management and control strategies for a HES connected in DC coupled architecture. The presented architecture can also be used for DC micro grids. Power management strategies are developed in a hierarchical architecture as an event driven finite state machine. Primary control is implemented using current mode control and voltage mode control adapted at the bi-directional DC-DC converters and the voltage source inverter connected to the HES, respectively. The performance of the developed power management strategies for the HES is analyzed for typical load dynamics.

Keywords: DC micro grid; standalone photovoltaic system; hybrid energy storage; power management; finite state machine

1. Introduction

Nearly one third of the world population is not electrified due to lack of generation, geographical, environmental and logistic concerns. Extending power lines from centralized sources to rural areas where electrification is embryonic is often not yet economical, and so, decentralized and off-grid power sources, such as standalone PV systems, are a promising alternative [1].

The intermittent and stochastic nature of PV production could be addressed by having an appropriate energy storage. When grid connected, if there is an imbalance of demand and the PV generation, the utility grid ensures an uninterruptible power supply to the load [2–4]. But unlike in grid-connected case, in standalone PV systems, any mismatch between the demand and PV generation should be compensated by the energy storage (ES) [5, 6]. Even with the grid connected case, there might be situations where grid is unavailable for supplying loads, (e.g., grid outage, islanding condition etc.) leading the PV system to be changed its working mode from grid connected to standalone [7]. Among many types of ES elements, chemical batteries are employed as mainstream long term ES solution for different kind of energy systems, particularly Lead Acid (LA) batteries with well proven technology due to its better electrical performance and relatively lower cost. Despite economical and electrical merits associated with LA batteries, the battery itself is not be an appropriate ES element in PV systems as the life cycle of LA battery is relatively short which only last for hundreds of charge-discharge cycles [8]. Due to the stochastic nature of PV generation, the deterioration of the LA battery could be worse as it fails to ensure charging and discharging security due to deep discharged, overcharging, high charging rate and fluctuating power exchange [8–10]. In order to address fast dynamics and sudden fluctuations in power intensive load (e.g., EV load, emergency power management), a super-capacitor(SC) should be embedded in the energy storage as it can absorb and deliver power fluctuations at much higher rates compared to batteries and also it can be considered that charging and discharging cycles of a SC is almost unlimited [5,8,11]. Therefore, it is recommended to use a battery with a SC as a hybrid ES (HES) in renewable energy applications to address its intermittency while ensuring long life cycle of the battery array.

A typical DC coupled active topology of a HES found in recent literature is depicted in Figure 1 where the battery array and SC are connected to a common DC bus [12–16]. A passive HES topology described in [17] can also share the load current between the battery and the SC while keeping the terminal voltage constant due to the parallel connection. In this topology, for fast dynamics in the load demand, the SC responses rapidly to satisfy the sudden changes in the demand which in consequence leads the battery current to gradually increase or decrease. However, in this topology, the individual power share can not be controlled independently unlike in the active topology illustrated in Figure 1, as the current distribution between the battery and SC solely depend on the internal electrical properties such as resistance, capacitance etc [13].

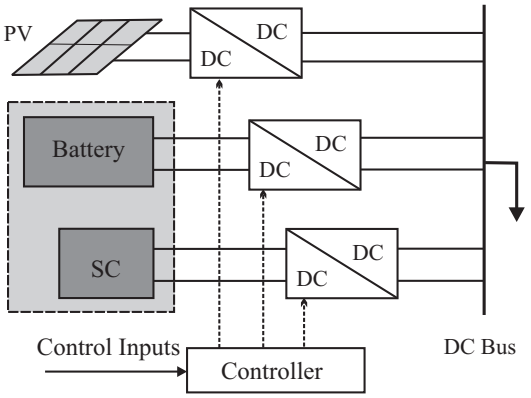

Figure 1. HES Topologies.

The power share among ES elements should be determined using appropriate techniques considering the characteristics of ESs. Independent control of the power flow of each energy storage element in a HES is useful, but to counter balance the system reliability and availability, secondary control layer would be necessary on top of the calculated power references. Reference [18] has employed fuzzy control to further modify and smooth the calculated power references for a HES but it has not given a significant attention to control strategies related to the voltage source inverter (VSI) in the SPVS application. Although considerable research efforts have been devoted to primary control of the power conditioning devices connected to the HES in a SPVS, less attention has been paid on the secondary control with energy management ensuring an uninterruptible power supply to the power intensive load with transients. Therefore, in this work, a hierarchical control approach as a finite state machine (FSM) is proposed and analyzed for the DC coupled HES in active topology. The initial power references for each ES element is calculated using power transient filtering. The control strategies are analyzed for both the DC-DC and DC-AC stages to ensure an uninterruptible power supply to the AC load while maintaining system reliability, availability and dispatching security.

In this article, Section 2 presents the configuration of the HES topology and the components. Section 3 describes the control strategies proposed as a FSM while the Section 4 is presenting the PWM switching control with classical PID control. The simulation results are presented and discussed in Section 5. The performance of the proposed control strategies are concluded in Section 6.

2. Topology of the HES components

In the presented work, ES elements are interfaced in DC coupled active topology to supply the power intensive load as depicted in Figure 2. Power shares of ES elements are determined using power transient filtering techniques. The energy sources are connected with the power intensive load through power conditioning devices with the control system as illustrated in Figure 2. The control system is developed in hierarchical fashion with dedicated control tasks at different stages to supply the required demand while ensuring charging and discharging security of the HES.

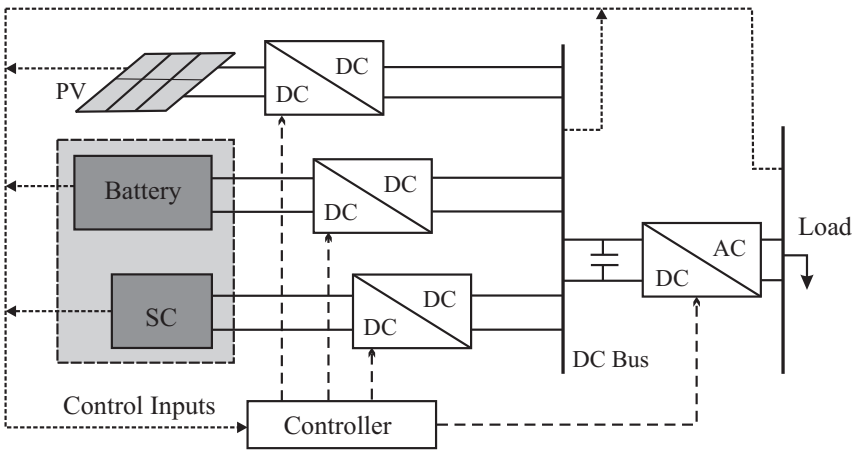

Figure 2. DC Coupled Architecture of the HES.

2.1. Lead-Acid battery model

The charging and discharging characteristics of the selected LA battery model are expressed in (2.1) and (2.2) respectively [19]. The sizing of the battery array is done based on the work presented in [9,20] with the power rating of 8 kW. The DC bus to which the battery is connected through a bi-directional DC-DC converter is kept at 60 V. The manufacture specified battery parameters are given in Table 1. According to the selected battery, the battery array consists of 7 batteries connected in parallel to meet the load demand.

$$E_{Charge} = E_0 - K \times \left(\frac{Q}{Q - it}\right) \times i^* - K \times \left(\frac{Q}{Q - it}\right) \times it + \mathcal{L}^{-1}\left(\frac{Exp(s)}{sel(s)}\right) \tag{2.1}$$

$$E_{Discharge} = E_0 - K \times \left(\frac{Q}{0.1Q + it}\right) \times i^* - K \times \left(\frac{Q}{Q - it}\right) \times it + \mathcal{L}^{-1}\left(\frac{Exp(s)}{sel(s)} \times \frac{1}{s}\right) \tag{2.2}$$

where,

E_0: Constant voltage (V)
$Exp(s)$: Exponential zone dynamics (V)
$sel(s)$: Battery mode: $sel(s) = 1$ during charging and $sel(s) = 0$ during discharging
K: Polarization constant (Ah^{-1}) or Polarization resistance (Ω)
i^*: Low frequency current dynamics (A)
i: Battery current (A)
it: Expected capacity (Ah)
Q: Maximum battery capacity (Ah)

Table 1. Battery parameters.

Parameters	Data
Nominal Voltage	48 V
Rated Capacity	69.4 Ah
Initial State of Charge	80%
Fully Charged Voltage	52.3 V
Nominal Discharge Current	35 A
Internal Resistance	0.02 Ω
Capacity at Nominal Voltage	21.5 Ah

2.2. Super-Capacitor model

SC is used to address the sudden power transients in the system rather taking a large portion of the load demand. However, the power rating of the SC should be large enough to address load transients and also SC should be capable of taking a significant share of the demand when the battery array is to be exceeded its power ratings.

The output voltage of the SC model used in this work is expressed using a Stern equation given in (2.3) [19]. The power ratings of the selected SC is 2.5 kW and the DC bus to which the SC is connected through a bi-directional DC-DC converter is kept at 60 V. The nominal voltage of the SC is selected as 24 V. The SC model parameters given in Table 2 [21].

$$V_{sc} = \frac{N_s Q_T d}{N_p N_e \varepsilon \varepsilon_0} + \frac{2N_e N_s RT}{F} \sinh\left(\frac{Q_T}{N_p N_e^2 A_i \sqrt{8RT\varepsilon\varepsilon_0}}\right) - R_{sc} i_{sc} \tag{2.3}$$

where,
$Q_T = \int i_{sc} dt$: Electric charge (C)

A_i: Inter-facial area between electrode and electrolyte (m^2)
F: Faraday constant (V)
i_{sc}: Super capacitor current(A)
V_{sc}: Super capacitor voltage (V)
N_e: Number of layers of electrodes
N_p, N_s: Number of parallel and series SCs
R: Ideal gas constant
T: Operating temperature (K)
ε, ε_0: Permitivity of material and the free space

Table 2. Super-capacitor parameters.

Parameters	**Data**
Rated Capacitance	96 F
Equivalent DC series resistance	2.1×10^{-3} Ω
Initial State of Charge	65%
Rated Voltage	36 V
Initial Voltage	24 V
Nuber of series capacitors	2
Number of parallel capacitors	4

2.3. Power conditioning devices

The system consists of two bi-directional DC-DC buck-boost converters and one 3ϕ VSI as power conditioning devices. In the HES system, both the bi-directional DC-DC buck-boost converters connected with the LA battery and SC arrays facilitate both charging and discharging modes as they are capable of handling bi-directional regulated power flow. The critical parameters of the DC-DC converters are calculated based on the methodology presented in [10]. As the DC coupled architecture is used in the HES, one VSI is employed with voltage mode control.

2.4. Control system overview

The power dispatching strategies are designed in hierarchical fashion as an event driven system with PID and state-flow control. Hierarchical control approach includes several hierarchical stages and each stage is responsible for doing a control task based on its hierarchical position. Therefore, the control system includes four stages each having their own control task depend on the hierarchical position as illustrated in Figure 3.

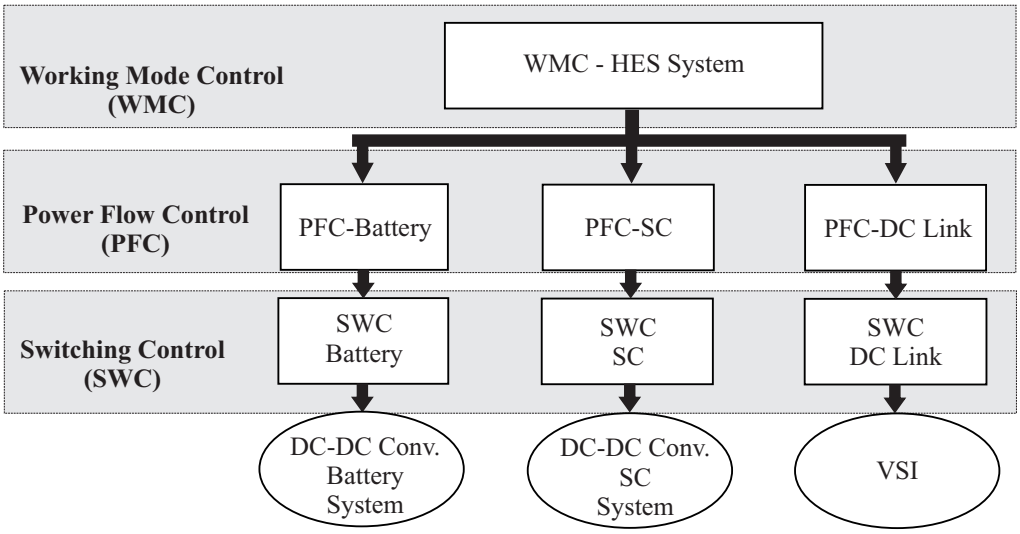

Figure 3. Hierarchical control structure.

3. Power management and switching control

The whole control task is subdivided into three hierarchical stages as illustrated in Figure 3. The top most working mode control (WMC) layer selects the suitable ES elements based on their availability and accessibility so that it prevents the ES elements from over charging and discharging by taking the prescribed maximum and minimum state of charge (SOC) limits of the battery into account. This layer determines the required power, frequency and voltage set points to meet the load demand. Power shares are determined at the power flow control (PFC) layer based on power transient filtering technique but the determined power references are further modified according to the power ratings and the discharging rates of the ES elements using event driven state-flow control. Based on the reference power signals calculated at the PFC, switching control (SWC) level generates the required PWM signals to converters.

3.1. Working mode control (WMC) of the system

At this stage, the availability and the accessibility of each ES element for power dispatching are determined based on their SOC. The control layer is designed as an event driven system with state-flow control. The state transition diagram of the WMC layer for the HES system is shown in Figure 4 and the corresponding state transition logic is tabulated in Table 3.

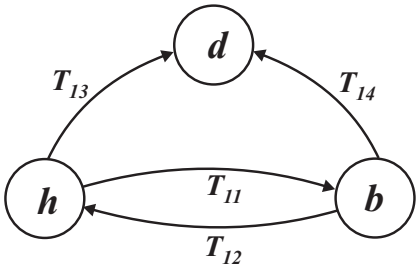

Figure 4. State transition diagram of the WMC layer.

h: Hybrid mode.
b: Battery only mode
d: Disconnected mode

Table 3. State transition logic of WMs.

Transition	Logic
T_{11}	$SOC_{bat}(t) > SOC_{bat,min}$ && $SOC_{sc}(t) < SOC_{sc,min}$
T_{12}	$SOC_{bat}(t) > SOC_{bat,min}$ && $SOC_{sc}(t) > SOC_{sc,min}$
T_{13}	$SOC_{bat}(t) < SOC_{bat,min}$ && $SOC_{sc}(t) < SOC_{sc,min}$
T_{14}	$SOC_{bat}(t) < SOC_{bat,min}$

$SOC_{x,min}$: minimum SOC of the ES element x
$SOC_x(t)$: current SOC of ES element x
x: battery-*bat*, SC-*sc*

3.2. Power Flow Control (PFC) of the HES

Power will be delivered to the load only in the 'Hybrid' and 'Battery only' modes. Power shares of each ES element will be determined by using linear filtering technique considering the load increment rate and the power transient frequency.

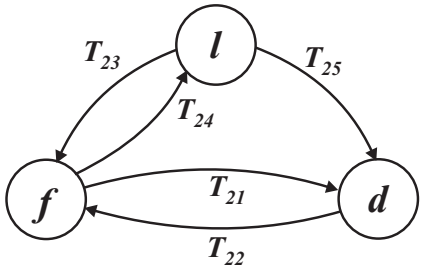

Figure 5. State transition diagram of the Hybrid mode in PFC.

The 'Hybrid'(h) mode in Figure 4 consists of three states (s) : 'Fully dispatchable'(f), 'Limited' (l) and 'Disconnected'(d) as illustrated in the state diagram of PFC (Figure 5).

There are only two states (s) : 'Connected'(c) and 'Disconnected'(d) in the 'Battery Only' mode. The state transition logic of PFC-Hybrid mode is tabulated in Table 4. Therefore, the final power references of the battery and SC for f and l states are calculated using (3.1) and (3.2), respectively. When the calculated battery power share using power transient filtering is higher than the maximum allowable capacity of the battery, the system transits to the l state where the initial power reference will be updated to a predetermined percentage (e.g., 0.8) of the calculated reference as described in (3.1).

Table 4. State transition logic of PFC-Hybrid.

Transition	Logic
T_{21}	$P_{max,sc} + P_{max,bat} < P_L(t)$
T_{22}	$P_{max,sc} + P_{max,bat} > P_L(t)$
T_{23}	$P_{bat}(t) > P_{max,bat}$ && $P_{sc}(t) < P_{max,sc}$
T_{24}	$P_{bat}(t) < P_{max,bat}$ && $P_{sc}(t) < P_{max,sc}$
T_{25}	$P_{sc}(t) > P_{max,sc}$

$P_{x,max}$: power rating of the ES element x
$P_x(t)$: calculated share of ES element x
$P_L(t)$: current load demand

$$P_{ref,bat,hyb}(t) = \begin{cases} P_{bat}(t) & ;\text{if } s = f \\ 0.8P_{bat}(t) & ;\text{if } s = l \\ 0 & ;\text{otherwise} \end{cases} \tag{3.1}$$

$$P_{ref,sc,hyb}(t) = \begin{cases} P_{sc}(t) & ;\text{if } s = f \\ P_L(t) - P_{ref,bat,dis}(t) & ;\text{if } s = l \\ 0 & ;\text{otherwise} \end{cases} \tag{3.2}$$

There are two states(s) in the PFC of the 'Battery only' mode :'Connected' (c) and 'Disconnected' (d) where only the battery array takes care of the load demand hence, sudden power fluctuations will not be addressed. The load is supplied as long as $P_{max,bat} > P_L(t)$ only, otherwise the system transits to d. Therefore, the final battery and SC power references for 'Battery only' states are calculated using (3.3) and (3.4), respectively.

$$P_{ref,bat,bo}(t) = \begin{cases} P_L(t) & ;\text{if } s = c \\ 0 & ;\text{otherwise} \end{cases} \tag{3.3}$$

$$P_{ref,sc,bo}(t) = 0 \tag{3.4}$$

However, the calculated final reference values of the battery and SC are further checked for the power ratings of each ES element before sending them to the SC layer where PWM switching signals are generated. Therefore, the final reference values for the battery and SC are obtained using (3.5) and (3.6), respectively.

$$P_{ref,bat}(t) = \begin{cases} P_{ref,bat,j}(t) & ;\text{if } P_{ref,bat,j}(t) \le P_{bat,max} \\ 0 & ;\text{otherwise} \end{cases} \tag{3.5}$$

$$P_{ref,sc}(t) = \begin{cases} P_{ref,sc,j}(t) & ;\text{if } P_{ref,sc,j}(t) \le P_{sc,max} \\ 0 & ;\text{otherwise} \end{cases} \tag{3.6}$$

$P_{ref,x,j}$: Power reference of x element in j mode — x: battery (*bat*), SC (*sc*),
$P_{x,max}$: Power rating of x element — j: hybrid (*hyb*), battery only (*bo*)

4. PWM switching control (SWC)

As illustrated in Figure 6, the attention is given to PWM switching controls of the power conditioning devices in the system. Basically what SWC layer does is generating the appropriate PWM switching signal to DC-DC bidirectional converters and the 3ϕ VSI for delivering the required power demand.

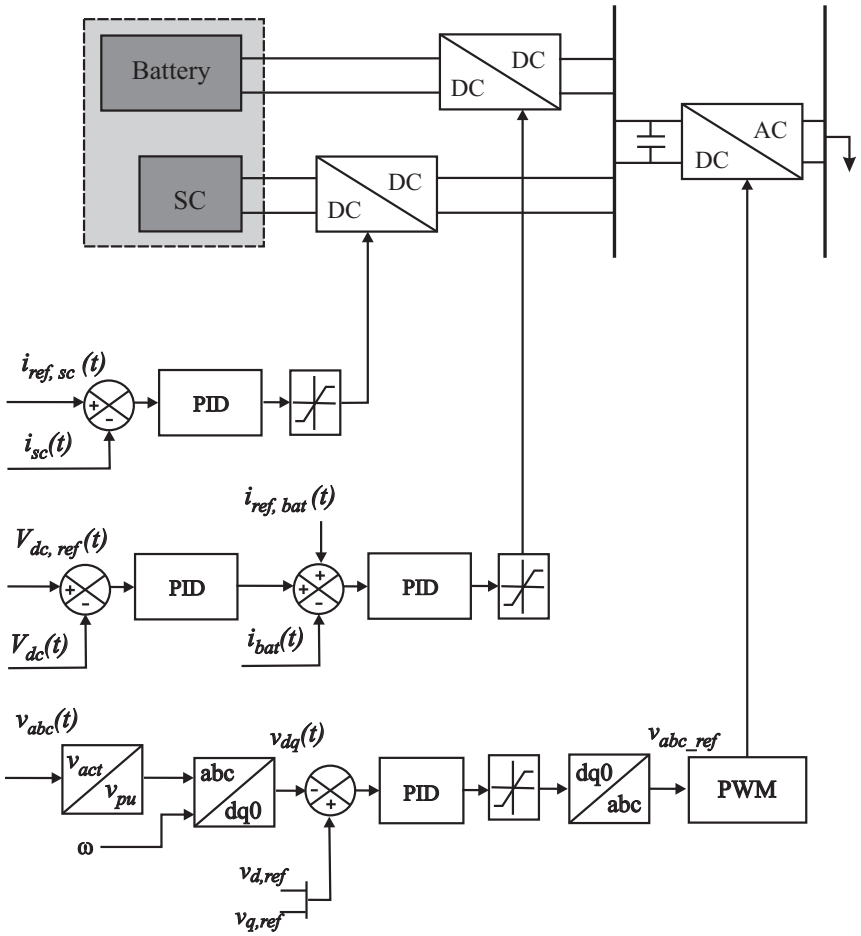

Figure 6. PWM switching control (SWC) system.

Individual power shares of each ES element is controlled using two PID control loops based on the reference values of the current components ($i_{ref,bat}$, $i_{ref,sc,}$) calculated from the corresponding power references ($P_{ref,bat}$, $P_{ref,sc,}$) received from the PFC layer. This classical PID control is described in [10]. To keep the DC link voltage constant, a cascaded voltage control loop is used with the battery array as the SC is dedicated for handling sudden power transients while supplying a share of the load demand. The 3ϕ VSI is controlled in grid forming mode using voltage mode control as the load management system is designed for a standalone application as illustrated in Figure 6. All the reference values ($v_{d,ref}$, $v_{q,ref}$ and f_{ref}) are obtained from the PFC layer to generate the required AC signal. The block diagram view and the control block diagram of the SWC topology used in the VSI connected with the DC link is shown in Figure 7.

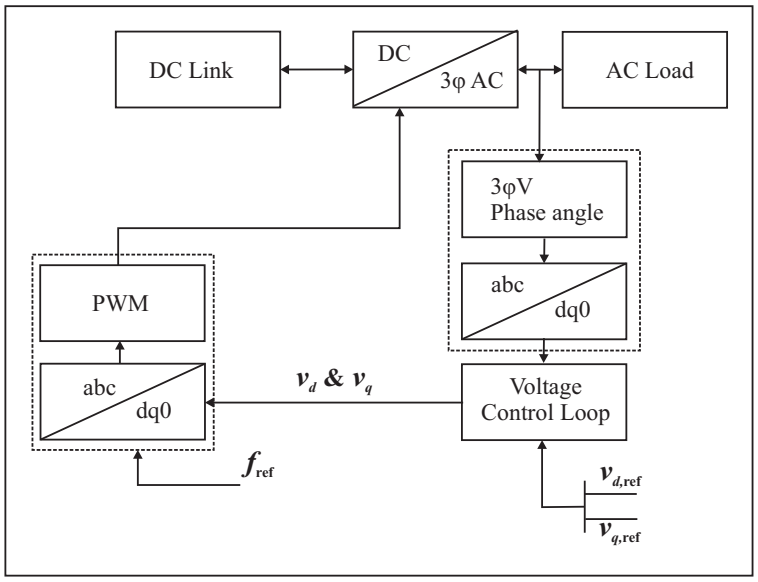

Figure 7. The block diagram of the SWC in the VSI.

There are two main subsystems: (1) Park component derivation subsystem (2) Voltage control subsystem, in the block diagram shown in Figure 7. The Park component derivation subsystem converts the measured line voltage wave-forms (v_{abc}) at the point of common cupping (PCC) with the AC bus into Park components (v_d, v_q) in *pu* values with the help of the phase angle (ωt). In this SWC topology, voltage controller is used to control the output voltage. Then in the SWC, the direct axis Park component of the reference voltage is set to 1 *pu* ($v_{d,ref} = 1$ *pu*) and it generates the required v_d, v_q for the PWM generation subsystem.

5. Results and discussions

The proposed control strategies of the HES are analyzed and the obtained results are presented for three scenarios where fast dynamic, slow dynamic and constant load profiles are considered, respectively. The load demand is properly shared between the battery and SC in the HES. The LA battery array is the main power source which takes the significant portion of the load demand while the SC is taking care of rapid dynamics of the power intensive load.

5.1. *Load demand sharing : Scenario-I-Load profile with rapid dynamics*

Demand management capability of the proposed HES architecture for a load profile with rapid dynamics is evaluated for the load profile illustrated in Figure 8. It can be seen that the large portion of the load demand is taken by the battery. System dispatches the power in 'Hybrid' mode and the power flow is taken place in both 'fully dispatchable' and 'limited' states.

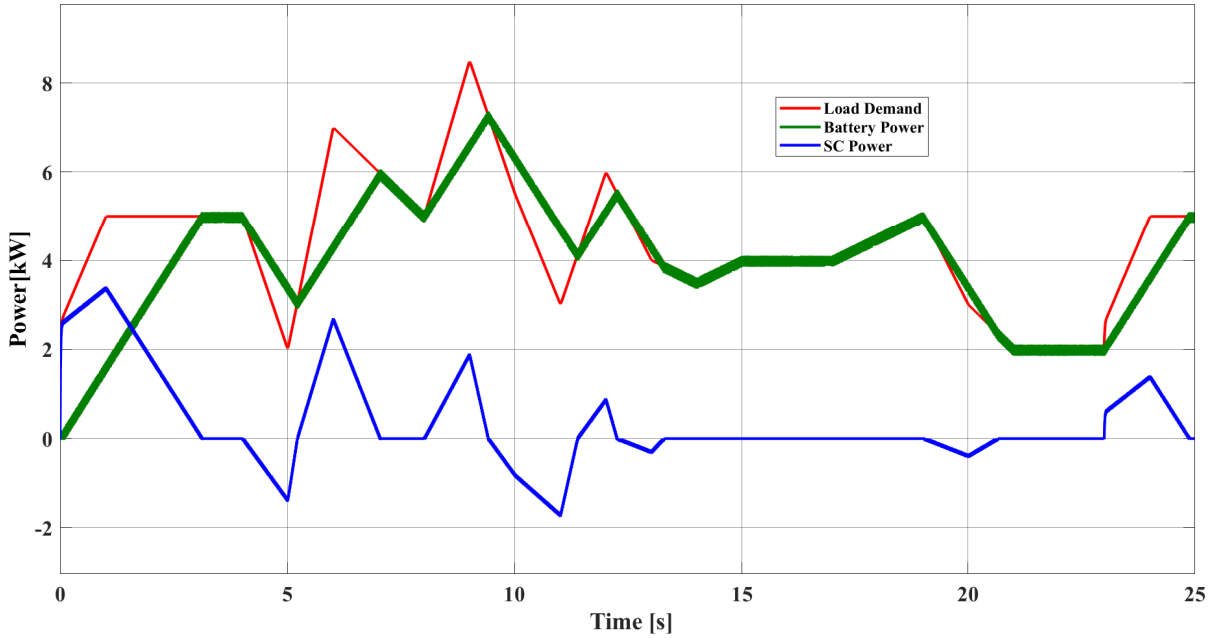

Figure 8. Variation of Power Shares of each ES Elements for Scenario I.

When we consider the load variation (Figure 8), rapid dynamics of the load demand can be seen during 4^{th} second to 13^{th} second. During the considered simulation time period, the peak demand of 8.5 kW has been occurred at the 9^{th} second. Out of this 8.5 kW demand, 23% is taken by the SC array while LA is taking 77%. From 8^{th} second to 9^{th} second, we can see a sudden increment of the load demand with a rate of 3.5 kW/s. During this period SC array has discharged power at a rate of 1.95 kW/s after being in rest, as the battery has failed to accomplish this sudden load change with alone. During this period the battery response is 1.55 kW/s which is not sufficient to meet this sudden demand change.

Similarly, during next two seconds ($9^{th}s - 11^{th}s$), a sudden demand decrement has been occurred which is even failed to addressed by the LA battery alone. During this time, load demand is decreased at a rate of 3.0 kW/s. SC array has suddenly disappeared at a rate of -3.9 kW/s while the LA battery keep discharging power at a rate of 1.55 kW/s. At the 10^{th} second, the share of battery discharge is 165% with respect to the load demand but, the excess energy is stored in the SC array at a rate of -2.2 kW/s during this rapid load change. The same discharging pattern continues till 11^{th} second resulting battery share of 4.9 kW and SC share of -1.9 kW at the $11^{th}s$.

The variation of the SOC, current and the terminal voltage of battery and SC for Scenario I are shown in Figure 9 and Figure 10, respectively.

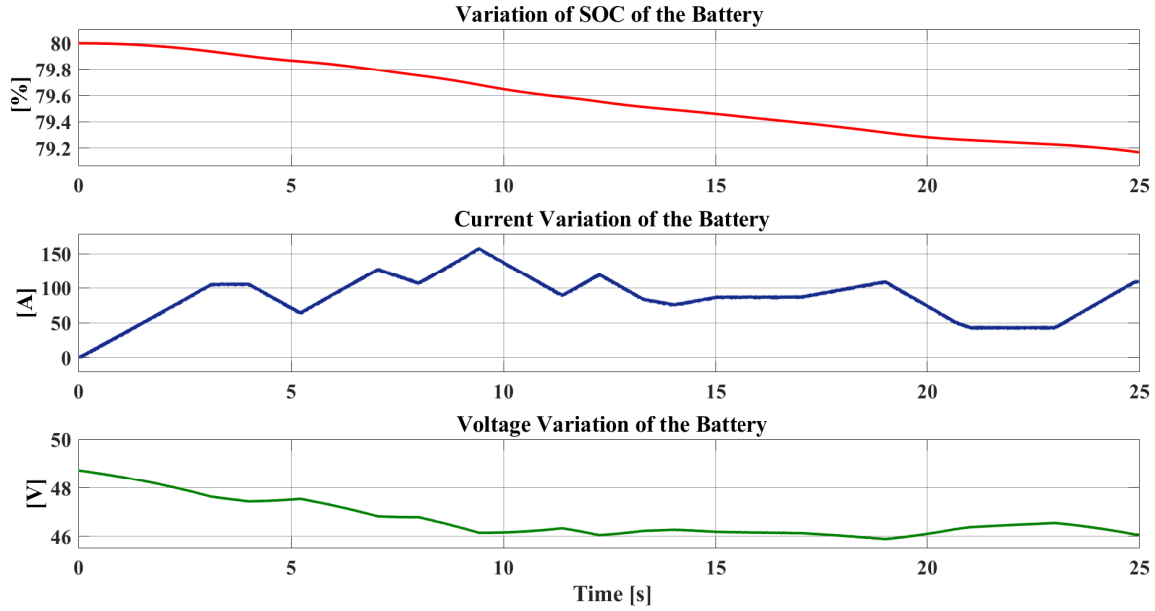

Figure 9. Variation of the Current, Voltage and SOC of the Battery for Scenario I.

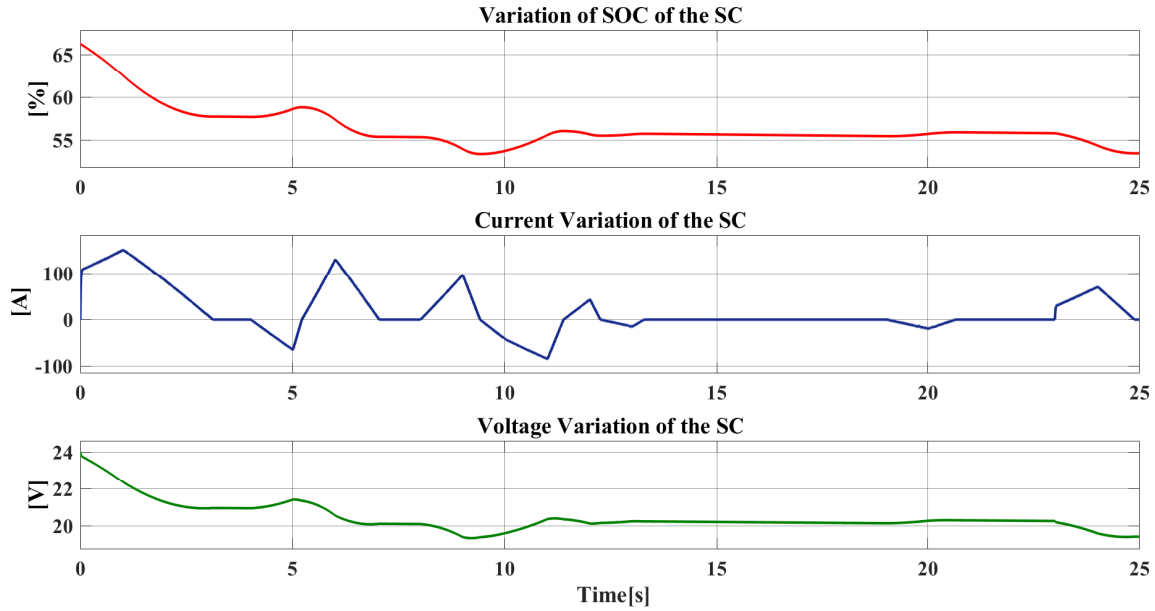

Figure 10. Variation of the Current, Voltage and SOC of the SC for Scenario I.

5.2. Load demand sharing : Scenario-II-Load profile with slow dynamics

System response for a load variation with slow dynamics is analyzed with the load profile illustrated in Figure 11. Similarly like in Senario I, the system dispatches the power in 'Hybrid' mode and the power flow is taken place in both 'fully dispatchable' and 'limited' states. As compared to the load variation in Senario I, very slow dynamics appear in the Senario II. Due to the rate limiter in the battery power management system, during the first and last few seconds, SC discharges to compensate the load demand and it can be seen that the load demand is almost fulfilled by the LA battery array in its 'fully dispatchable' state.

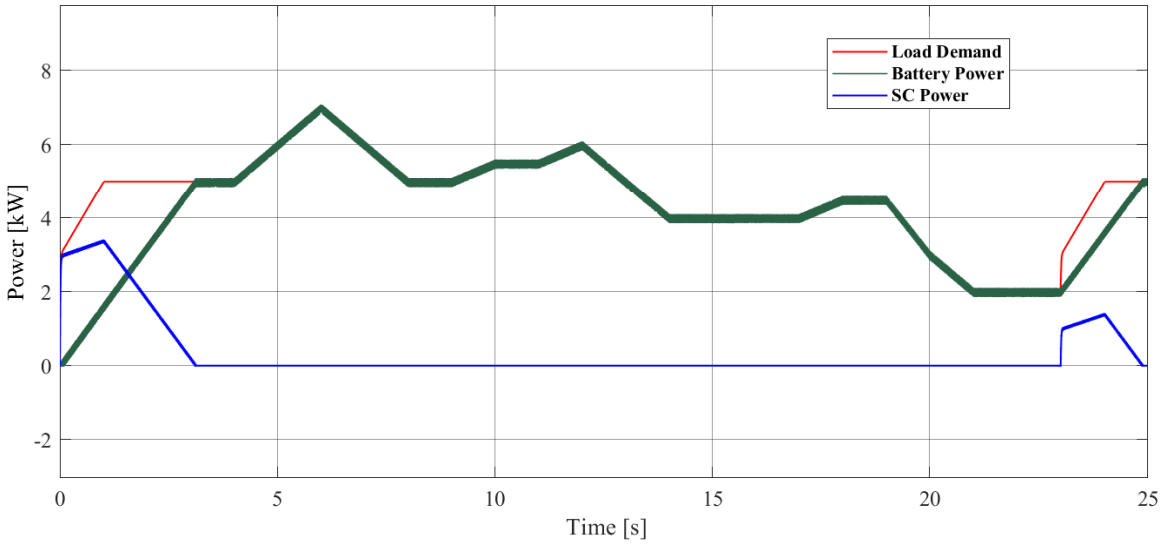

Figure 11. Variation of Power Shares of each ES Elements for Scenario II.

The variation of the SOC, current and the terminal voltage of battery and SC for Scenario II are shown in Figure 12 and Figure 13, respectively.

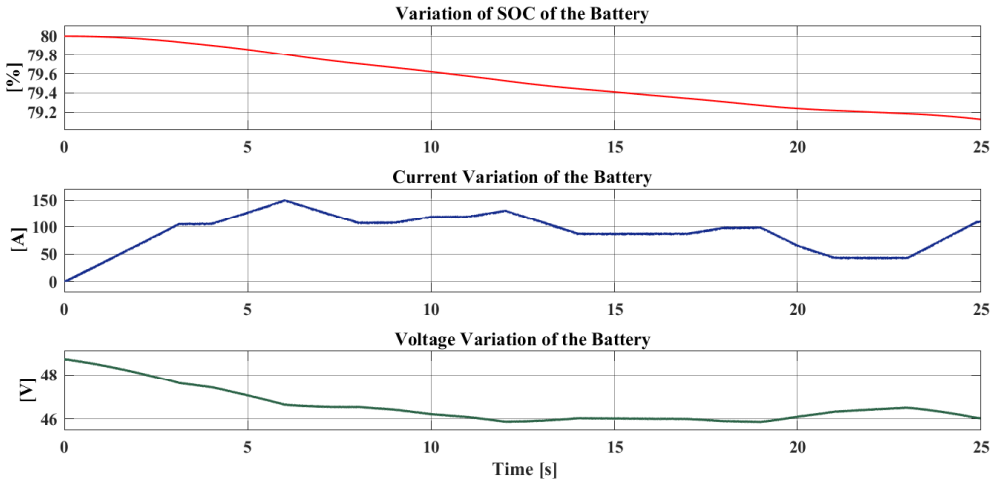

Figure 12. Variation of the Current, Voltage and SOC of the Battery for Scenario II.

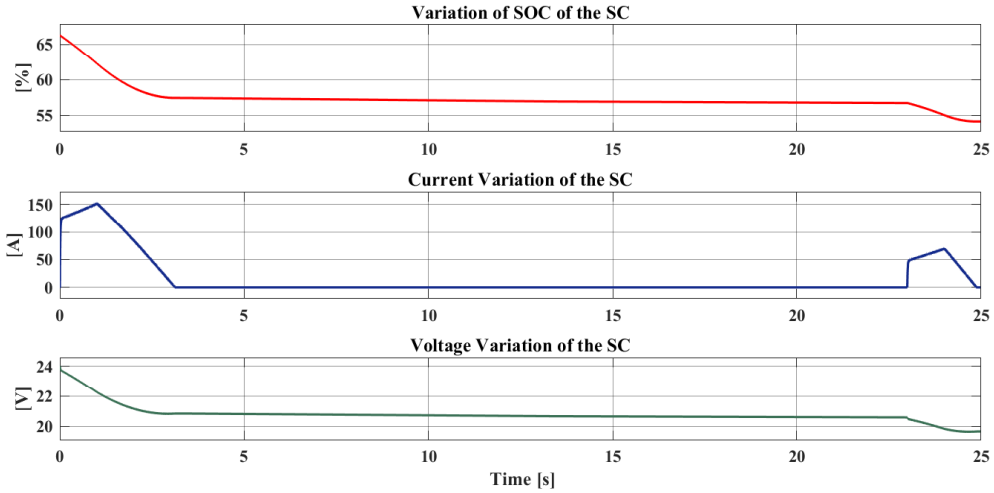

Figure 13. Variation of the Current, Voltage and SOC of the SC for Scenario II.

5.3. Load demand sharing: Scenario-III-Constant load profile

To analyze the performance of proposed power management strategies for 'Battery only' mode, a constant load profile is considered as shown in Figure 14. When the SC array is not available for power dispatching, power transients can not be handled. Therefore, either constant load or a load with very slow dynamics can only be handled in 'Battery only' mode.

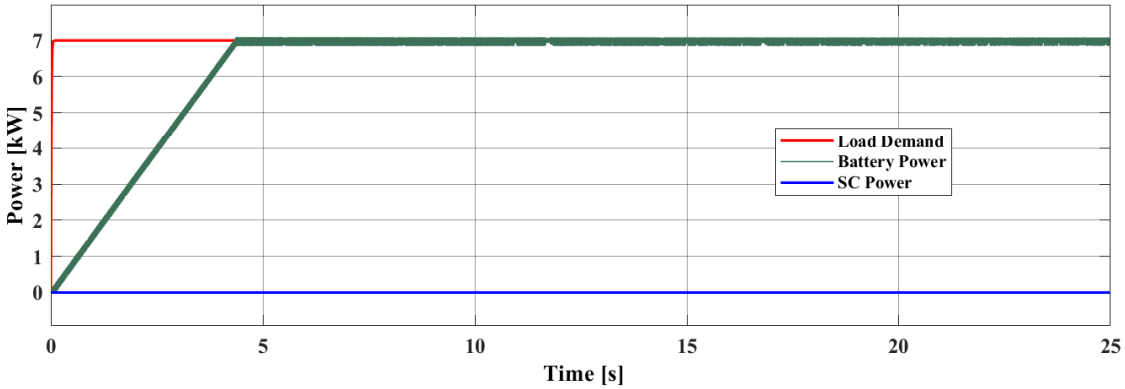

Figure 14. Variation of Power Shares of each ES Elements for Scenario III.

In Scenario-I, it can be seen that the transients of the load profile are filtered and compensated by the SC. The system is working in the *h* mode and both *f* and *l* states. Very slow dynamics are appearing in the load profile analyzed in Scenario-II, and so, the load demand is taken by the LA battery array. At the start and the end, SC has taken a power share of the load, as the system has switched to *l* state of the *h* mode during those periods. To analyze the performance of control strategies proposed in *b* mode, the constant load profile is considered in the Scenario-III, and it can be seen that, as long as the battery array is available, the constant load profile can be supplied by the system.

6. Conclusions

In standalone energy systems as well as in islanding mode of the grid connected PV systems, LA batteries serve as the long term energy storage by taking large portion of the load while sudden changes are being handled by a SC array embedded with the LA battery as a hybrid energy storage. It can be seen that the given HES architecture with the proposed control strategies developed in hierarchical manner effectively address the fast dynamics of the load demand without stressing the LA battery. Power dispatching strategies are developed by using current mode control and voltage mode control adapted at the bi-directional DC-DC converters and the voltage source inverter of the proposed HES with the help of state flow based event driven and PID control systems. Rather using only primary control for the power conditioning devices, it is very effective to implement logical control on top of the primary switching control in hierarchical manner to maintain smooth power supply to the load ensuring healthy operation.

In this work, the power shares determined by using the power transient filtering technique are further modified by considering the availability and accessibility of each power source to ensure an uninterruptible power supply to the load. It could be concluded that the proposed architecture and the control strategies for a HES connected in DC coupled nature helps not only in increasing more utilization of battery power to meet the rapid varying load demand but also in improving system dynamics and stability in addition to enhance the life expectancy of LA battery.

This proposed HES system with control strategies can be directly used for fast charging of EV without stressing the electrical grid and also which is best suited for industrial drives as well. The presented power dispatching topology is going to be very useful for emergency power management using HES during disaster relief efforts. In future works, this work will be extended to a PV based DC micro-grid with both dispatching and changing control.

Acknowledgments

This work is partially supported by the Norwegian Ministry of Foreign Affairs through the Royal Norwegian Embassy, New Delhi under the framework agreement with TERI (India) and University of Agder (Norway) for the project theme ‘Sustainability and Clean Energy’.

Conflict of interest

The authors declare no conflict of interest in this paper.

References

1. Kolhe M (2009) Techno-Economic optimum sizing of a Stand-Alone solar photovoltaic system. *IEEE Trans Energy Convers* 24 : 511–519.
2. Wu Y, Lin J, Lin H (2017) Standards and guidelines for Grid-Connected photovoltaic generation systems: A review and comparison. *IEEE Trans Ind Appl* 53: 3205–3216.

3. Collins L, Ward JK (2015) Real and reactive power control of distributed PV inverters for overvoltage prevention and increased renewable generation hosting capacity. *Renewable Energy* 81: 464–471.
4. Blaabjerg F, Teodorescu R, Liserre M, et al. (2006) Overview of control and grid synchronization for distributed power generation systems. *IEEE Trans Ind Electron* 53: 1398–1409.
5. Thang TV, Ahmed A, Kim C, et al. (2015) Flexible system architecture of Stand-Alone PV power generation with energy storage device. *IEEE Trans Energy Convers* 30: 1386–1396.
6. Zhou W, Lou C, Li Z, et al. (2010) Current status of research on optimum sizing of stand-alone hybrid solar-wind power generation systems. *Appl Energy* 87: 380–389.
7. Lu D, Fakham H, Zhou T, et al. (2010) Application of Petri nets for the energy management of a photovoltaic based power station including storage units. *Renewable Energy* 35: 1117–1124.
8. Jing WL, Lai CH, Wong WSH, et al. (2016) Cost analysis of battery-supercapacitor hybrid energy storage system for standalone PV systems. *4th IET Clean Energy and Technology Conference (CEAT 2016)*, Institution of Engineering and Technology.
9. Yassin MAM, Kolhe ML, Azmi AN (2017) Battery capacity estimation for building-integrated photovoltaic system: Design study of a Southern Norway ZEB house. *2017 IEEE PES Innovative Smart Grid Technologies Conference Europe (ISGT-Europe),* 1–6.
10. Konara KMSY, Kolhe ML (2016) Charging management of grid integrated battery for overcoming the intermittency of RE sources. *2016 IEEE International Conference on Information and Automation for Sustainability (ICIAfS)*, IEEE.
11. Fakham H, Lu D, Francois B (2011) Power control design of a battery charger in a hybrid active PV generator for Load-Following applications. *IEEE Trans Ind Electron* 58: 85–94.
12. Choi M, Kim S, Seo S (2012) Energy management optimization in a battery/supercapacitor hybrid energy storage system. *IEEE Trans Smart Grid* 3: 463–472.
13. Etxeberria A, Vechiu I, Camblong H, et al. (2012) Comparison of three topologies and controls of a hybrid energy storage system for microgrids. *Energy Convers Manage* 54: 113–121.
14. Wongdet P, Marungsri B (2018) Hybrid energy storage system in standalone DC microgrid with ramp rate limitation for extending the lifespan of battery. *2018 International Electrical Engineering Congress (iEECON)*, 1–4.
15. Sinha S, Sinha AK, Bajpai P (2017) Solar PV fed standalone DC microgrid with hybrid energy storage system. *2017 6th International Conference on Computer Applications In Electrical Engineering-Recent Advances (CERA)*, 31–36.
16. Deshpande G, Kamalasadan S (2014) An approach for micro grid management with hybrid energy storage system using batteries and ultra capacitors. *2014 IEEE PES General Meeting-Conference Exposition*, 1–5.
17. Dougal RA, Liu S, White RE (2002) Power and life extension of battery-ultracapacitor hybrids. *IEEE Trans Compon Packag Technol* 25: 120–131.
18. Liu B, Zhuo F, Bao X (2012) Fuzzy control for hybrid energy storage system based on battery and Ultra-capacitor in Micro-grid. *Proceedings of The 7th International Power Electronics and Motion Control Conference* 2: 778–782.

19. The Mathworks, Inc., Natick, Massachusetts, *MATLAB version 9.5 (R2018b)*, 2018.

20. Yassin MAM, Kolhe M, Sharma A, et al. (2017) Battery capacity estimation for building integrated photovoltaic system: Design study for different geographical location(s). *Energy Procedia* 142: 3433–3439.

21. Azmi AN, Kolhe ML (2015) Photovoltaic based active generator: Energy control system using stateflow analysis. *2015 IEEE 11th International Conference on Power Electronics and Drive Systems*, 18–22.

AIMS Press